Chapter 17
Towards Modeling of Metabolic Syndrome: Tissue Crosstalk in Lipid Spillover

Sergey Smirnov, Eugeny Metelkin, Nail Gizzatkulov, Oleg Stepanov and Oleg Demin

Abstract In this chapter we propose a framework for development of the mathematical model of Metabolic Syndrome. The cornerstone of the model is "adipose tissue expandability hypothesis", which treats long-term increase in FAs concentration in blood and their subsequent accumulation in muscle and liver as a main cause of decrease in insulin sensitivity and, consequently, MetS development. The key biological facts underlying the construction of MetS model have been collected and analyzed and the main requirements of the model have been formulated. To take these facts into account and meet the requirements formulated, we have developed a novel algorithm enabling us to combine kinetic models, which describe changes in metabolite (lipoproteins) concentrations due to biochemical transformations in blood and tissues, with the mathematical model of the molecular movement in blood flow.

Keywords Lipid metabolism · Lipid spillover · Kinetic modeling · Very low density lipoprotein

17.1 Introduction

Metabolic syndrome (MetS) develops through a long and complex process, which is associated with several organs and tissues. Several experimental data values characterizing various aspects of MetS have been simulated and collected. However, mathematical models describing the development of MetS, and for example, its progression to type 2 diabetes (T2D), have not yet been developed. To a large extent, this is due to the inherent complexity of the processes and regulatory mechanisms related to MetS. To correctly describe the development of MetS, a mathematical model needs to account for the crosstalk between different organs and tissues at various levels such as physiological and biochemical levels.

S. Smirnov (✉) · E. Metelkin · N. Gizzatkulov · O. Stepanov · O. Demin
Institute for Systems Biology SPb, Leninskie Gory 1/75, Moscow, Russia, 119992
e-mail: smirnov@insysbio.ru

M. Orešič, A. Vidal-Puig (eds.), *A Systems Biology Approach to Study Metabolic Syndrome,* 341
DOI 10.1007/978-3-319-01008-3_17,

One of the main factors in MetS development is a decrease in tissue sensitivity to insulin (Albu et al. 2010; Felber and Golay 2002; Golay et al. 1984; He et al. 2010; Lin et al. 2009; Muscelli et al. 2008; Pastucha et al. 2010; Pigeon et al. 2009). We use this fact as a basis for our MetS model. However, to construct such a model we first need to identify an experimentally confirmed mechanism that would allow us to establish the relationship between obesity and a decrease in insulin sensitivity (Czech et al. 2010; Katz et al. 2000; Prentki and Madiraju 2011; Stannard and Johnson 2004; Wu et al. 2010).

The aim herein is to outline a framework for further development of the mathematical model describing the occurrence of MetS and its progression to T2D within the conceptual framework of the adipose tissue expandability hypothesis (AEH) (Chap. 1.1). For this purpose, first, we developed a model to describe lipid spillover, which is the non-homogeneous concentration of fatty acids (FA) and lipoproteins in the circulatory system. To account for the space-time distribution of FAs and lipoproteins, we developed a new approach that allows us to combine models describing intra- and extra- cellular processes of biomolecules and lipoprotein particle transformation, where the models describe the transport of blood, molecules, and lipoproteins in the circulatory system.

17.2 Modeling Framework: Description of the Biological System and Model Requirements

Based on AEH, the development of MetS can be associated with obesity and it consists of the following events.

In the first stage of the development of obesity, we assume that the expandability of the adipose tissue is high. This means that excess FAs can be stored in adipose tissue. The term “excess FA” refers to all FAs that originate in consumed food or are produced from glucose in the liver but have not been utilized in energy production. As obesity develops (i.e., patient weight increases), the expandability of adipose tissue decreases. If the energy supply resulting from food intake continues to be higher than the energy consumption required to sustain the organism, then the rate of influx of FAs starts to exceed the rate of FA storage in adipose tissue. This causes the concentration of FAs in the blood to increase and FAs to accumulate in certain tissues such as those of the muscle and liver. Accumulation of FAs in these tissues results in a decrease in their sensitivity to insulin. Muscle cells can utilize both glucose and FAs to produce the energy required to maintain intracellular processes and performance. This means that an increase in FA concentration may result in a decrease in glucose consumption, and as a consequence, a decline in the insulin-dependent transport of glucose in muscles.

Thus, to develop a model that satisfactorily describes MetS on the basis of AEH, we need to account for the following aspects of the disease (Armoni et al. 2007; Bajaj

et al. 2002; Everett-Grueter et al. 2006; Hirasawa et al. 2005; Kelley and Mandarino 2000; Kim et al. 2007; Lewis et al. 2002; Schnell et al. 2007; Staehr et al. 2003):

(i) transformation of glucose in the organism
(ii) lipid spillover
(iii) energy balance in the organism
(iv) tissue crosstalk underlying the interconnections between (i), (ii), and (iii).

Transformation of glucose in an organism. Glucose entering the organism through food can either be utilized to produce energy or it can be stored as glycogen in liver and muscle tissues and as FAs in adipose tissue. If glucose uptake exceeds glucose utilization for energy production over a long period, then all excess glucose is transformed into FAs, which are then stored in adipose tissue. The alternative method of glucose storage (as glycogen) cannot compete with the process of glucose transformation into FAs since the glycogen storage capacity of liver and muscle tissues is extremely low. This means that the ability to accumulate excess glucose in the form of glycogen is quickly weakened.

If the rate of glucose uptake exceeds the sum of the rates of (i) glucose consumption to produce energy and (ii) glucose transformation into FAs, then the glucose level in blood increases until it is balanced with the glucose clearance in urine. If the dominance of glucose intake over total glucose consumption occurs over a long period, then the glucose level in blood remains considerably high all the time. This is the main symptom of MetS (or T2D). In conclusion, we can state that MetS (or T2D) is a long-lasting state of an organism when the glucose intake rate permanently exceeds the total rate of its consumption to produce energy, resulting in the storage of glucose as FAs in adipose tissue.

Lipid spillover. Chap. 2.6 describes in detail the processes involved in FA transformation, transport, and homeostasis. Based on this description, we conclude that the fate of FAs entering the organism is highly similar to that of glucose. FAs can either be utilized to produce energy or be stored in adipose tissue. If the rate of FA uptake exceeds the sum of the rates of (i) FA consumption to produce energy and (ii) FA storage in adipose tissue, then the FA level in blood increases, i.e., excess FAs are observed. In accordance with AEH, excessive amounts of FAs in the organism are responsible for the development and progression of MetS.

In the version of the model presented below, we neglect many aspects of lipid spillover that are described in Chap. 2.6. For example, we do not distinguish between VLDL1 and VLDL2 and we do not take into account that there are other lipoproteins involved in lipid spillover, such as IDL and HDL.

Requirements for development of MetS model. Based on the description of the biological system presented above, we can prepare a list of requirements for the development of the MetS model, as follows:

- The model should reproduce the transport of glucose and FAs between different organs and tissues through biological fluids (tissue crosstalk).
- The model should reproduce glucose and FA dynamics for different diet and food intake regimens.

- The model should reproduce the dynamics of the glucose and FA exchange that is dependent on the energy balance (difference between the energy from consumed food and that utilized to meet energy needs) in the organism.
- The model should describe changes in the glucose and FA blood concentration levels resulting from the passage of blood through a selected organ/tissue (or part of the organ/tissue).

17.3 Model Development

As we have indicated in previous sections (see also Chap. 2.6), the main items considered in the MetS development model are the glucose and the FAs attached to various carriers. This means that the model development can be subdivided into three stages:

- development of the lipid spillover model
- development of the glucose homeostasis model
- merging of the lipid spillover and glucose homeostasis models

In this section, we describe the development of the lipid spillover model. Development of the glucose homeostasis model is not presented in this chapter. In accordance with the description in Chap. 2.6, there are several organs/tissues actively involved in lipid spillover. These are the liver, gastrointestinal tract, blood, muscles, and adipose tissue. Underlying lipid spillover is the intensive crosstalk between organs and tissues. The term "tissue crosstalk" refers to the mechanism by which one organ/tissue can influence the operation of another organ/tissue via excretion and transport of active components that can be absorbed and metabolized by the target organ/tissue. Tissue crosstalk is necessary for the cooperation between tissues, which results in homeostasis of glucose and FAs in an organism. The following types of crosstalk are involved in lipid spillover: *liver-adipose*, *liver-muscle*, and *adipose-muscle*.

To be able to describe tissue crosstalk and meet all the requirements discussed above, the MetS model should consider the complete organism as a set of compartments that exchange biological fluids (e.g., blood and lymph) and consist of biological entities (e.g., lipoproteins, molecules, and cells).

To build the compartmental structure, we define a "route" as a set of compartments that are sequentially located. Each route corresponds to a set of blood vessels located in an organ or part of an organ and describes the blood flow through the organ without branching or merging into the bloodstream.

A route is characterized by the following basic features:

- blood flow velocity along the route (i.e., the volume of the blood passing through the route per unit time)
- total volume of blood in a route (i.e., the sum of blood volumes in all compartments of the route at any given time)
- diameter of the blood vessels along the route

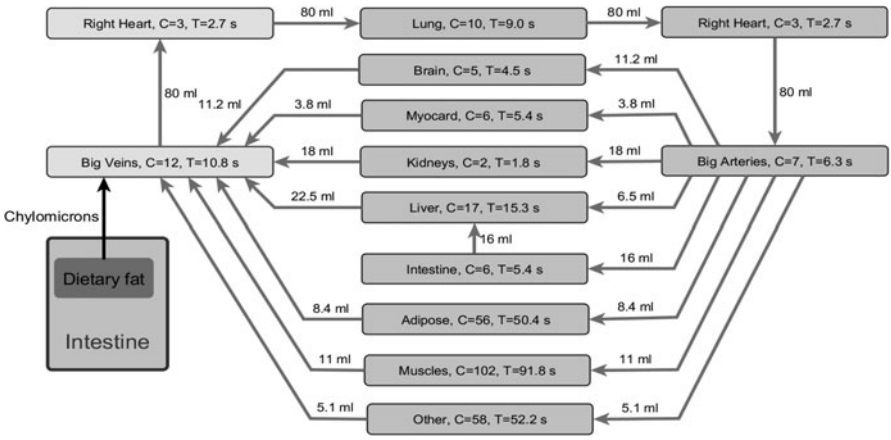

Fig. 17.1 Schematic of routes taken in lipid spillover model (physiological module). The circulatory system routes in the lipid spillover model are represented in this schematic. The number above each arrow indicates the volume of blood traveling through the routes per second (i.e., per cardiac beat). The following information is indicated in the rectangles: (i) name of the route, (ii) number of compartments included in the route (C), and (iii) residence time of the blood portion in the route (T)

On the basis of these characteristics, we can calculate the residence time of the blood in the compartments of a route. The residence time is equal to the ratio of the total volume of blood in the route and the blood flow velocity along the route.

The number of compartments in a route should be selected such that it is possible to reproduce both the anatomical location of various organs/tissues in an organism and their linkage via the circulatory system. Further, there should be a sufficient number of compartments to enable a detailed description of the space-time distribution of the biological entities (lipoproteins, molecules, or cells) along the route. Moreover, the number of compartments should be kept as low as possible to reduce the complexity of the model. To meet these requirements, we selected a compartment volume such that the blood residence time of the compartment was equal to one second. Therefore, the number of compartments in a route is equal to the blood residence time of the route, expressed in seconds. However, since the residence time and total blood volume differ for each route, the number of compartments and their volumes also differ.

Splitting the circulatory system into a set of routes is based on a specific biological task, and therefore, it changes for each model. The route schematic for the lipid spillover model is given in Fig. 17.1. A detailed description of the routes is presented in Table 17.1.

To model biochemical reactions that occur in either biological fluids (blood or lymph) or various organs/tissues interconnected via the circulatory system, we developed the step-by-step algorithm (SBSA). Within the framework of this algorithm, movement of blood along the route is combined with changes in concentrations of transported biological entities (molecules and lipoproteins), which is a result of

Table 17.1 Routes and compartment structure of model

Route	Model #	Number of compartments	Compartment volume (ml)	Transient time (sec)	Total blood volume in route (ml)
Right heart	No model [a]	3	80	2.7	240
Lung	No model [a]	10	80	9	800
Left heart	No model [a]	3	80	2.7	240
Big arteries	No model [a]	7	80	6.3	560
Brain	No model [a]	5	11.2	4.5	56
Myocard	Model 3	6	3.8	5.4	22.8
Kidneys	No model [a]	2	18	1.8	36
Liver	Model 4	17	22.5	15.3	382.5
Intestine	No model [a]	6	16	5.4	96
Adipose	Model 2	56	8.4	50.4	470.4
Muscles	Model 3	102	11	91.8	1122
Other	No model [a]	58	5.1	52.2	295.8
Big veins	Model 1	12	80	10.8	960

[a] "No model" means that only transfer of molecules with blood flow without any chemical transformation occur in these organs. Therefore, any kinetic model was not defined for these organs

chemical reactions and interactions at the walls of the blood vessels, in the following manner:

- Blood movement along a route is divided into discrete steps. The duration of each step corresponds to the blood residence time in a compartment.
- For the duration of a single step, blood is considered an immovable fluid. Changes in concentrations of biological entities in the selected compartment result from biochemical reactions and interactions at cells of only the vessel wall.
- At the end of a single step, the content of the *i-th* compartment is transported infinitely fast to the *(i + 1)-th* compartment. This is continued in subsequent steps.

Physical implementation of SBSA In this subsection, we focus on a system that can be represented by a network of interconnected compartments with fluid flowing through them. In this system, there are molecules (or particles), which can (1) react with each other in accordance with stoichiometry and reaction rates, (2) interact with immovable parts of the system (for example, the compartment walls), and (3) be transferred from one compartment to another with the fluid.

As a model of fluid flow, we consider an incompressible fluid that fills the complete volume of the compartments and has a laminar flow. Each point in the fluid flows at the same rate. The equation describing changes in metabolite (particle) concentrations in compartment ***s*** can be written as

$$\frac{\partial \overline{C}_s}{\partial t} + r_s \frac{\partial \overline{C}_s}{\partial x} = \widehat{N}_s \overline{v}_s + \overline{u}_s \tag{17.1}$$

Here, $\overline{C}_s$ is the vector of metabolite concentrations, r_s is the flow rate through the compartment ***s*** (if there is no flow in a compartment, then r = 0), $\widehat{N}_s$ is the stoichiometric matrix, $\overline{v}_s$ is the vector of reaction rates, $\overline{u}_s$ is the vector of the influxes of

molecules/particles from outside (for example, drug administration), t is time, and x is the variable describing the transfer along the compartment(s) resulted from the flowing fluid. The boundary condition describing the junction between compartments can be written as

$$r_s \frac{\partial \overline{C}_s}{\partial x}(0,t) = \sum\nolimits_j r_j \frac{\partial \overline{C}_j}{\partial x}(x_{\max,\mathrm{j}}, t) \tag{17.2}$$

where index j corresponds to all compartments that supply the flowing fluid to compartment $\boldsymbol{s}$. This boundary condition imposes the law of conservation of molecules/particles at the border between each compartment. The law of conservation of flowing fluid is given by

$$r_s = \sum_j r_j$$

Thus, the mathematical model (described by Eqs. 1 and 2) represents a set of advection equations interconnected with boundary conditions describing the continuity of the flowing fluid and the topology of the linked compartments.

To solve the system numerically, we have (1) assumed that the characteristic time for chemical reactions is much less than that of fluid transfer and (2) used an upwind differencing scheme for the construction of finite difference equations on the basis of differential equations (1 and 2).

We subdivide each compartment into smaller parts, allowing us to neglect the concentration gradient of volume $\Delta \mathrm{x} = \mathrm{V}_f$ where V_f is the fixed volume of the sub-compartment. Using the selected difference scheme, we obtain

$$\frac{\partial \overline{C}_s}{\partial x} \approx \frac{\overline{C}_f - \overline{C}_{f-1}}{V_f} \tag{17.3}$$

Where f is the index of the current sub-compartment of compartment s. Taking into account Eq. 1 and the boundary condition (Eq. 2), we arrive at

$$\frac{d\overline{C}_f}{dt} = -r_f \frac{\overline{C}_f}{V_f} + \sum\nolimits_i r_i \frac{\overline{C}_i}{V_i} + \widehat{N}_f \overline{v}_f + \overline{u}_f \tag{17.4}$$

where $\overline{C}_f$ is the function/variable, which depends on time only and index $\boldsymbol{i}$ corresponds to all compartments that supply the flowing fluid to compartment $\boldsymbol{f}$.

The value of $\overline{C}_f$ for each iteration of k is calculated in two stages: (1) we solve the system of equations without taking into account the contribution of fluid transfer and (2) we introduce corrections, which describe the contribution of the flowing fluid to changes in the concentrations of molecules/particles as well as the contributions from external sources.

The first stage describes the system without any influxes from other compartments:

$$\frac{d\overline{C'_f}}{dt} = \widehat{N}_f \overline{v}_f + \overline{u}_f \tag{17.5}$$

$$\overline{C'_f}(0) = \overline{C}_{f,k'} \tag{17.6}$$

These equations describe the chemical transformation of molecules/particles in the system but do not account for the contribution of their transfer with flowing fluid from one compartment to another. Concentrations of molecules/particles calculated in the previous iterations are taken as initial conditions. These equations give us the following solution at any small time period (ΔT):

$$\overline{C'_{f,k+1}} = \overline{C'_f}(\Delta T)$$

The second stage is to correct the solution derived in the first stage for the contribution of the flowing fluid:

$$\frac{\overline{C}_{f,k+1} - \overline{C'_{f,k+1}}}{\Delta T} = -r_f \frac{\overline{C'_{f,k+1}}}{V_f} + \sum\nolimits_i r_i \frac{\overline{C}'_{k+1i}}{V_i} \tag{17.7}$$

Hence,

$$\overline{C}_{f,k+1} = \overline{C}'_{f,k+1} - r_f \frac{\overline{C'_{f,k+1}}}{V_f} \Delta T + \sum\nolimits_i r_i \frac{\overline{C}'_{i,k+1}}{V_f} \Delta T \tag{17.8}$$

Mathematical implementation of SBSA As a mathematical object, the complete system can be represented as a series of compartments interconnected by edges. The compartments are split into routes that correspond to different organs (see Table 17.1). The edges are described by numeric characteristics that describe the movement between compartments in terms of a table of interconnections. The biological processes in each compartment are described by a kinetic model. Different compartments can be associated with the same or a different kinetic model.

The movement of blood and biological entities located in a specific portion of the blood is described in a pulse manner with a period equal to ΔT. It is assumed that the movement of the blood between neighboring compartments happens instantaneously at the end of the time period. This allows us to separate the solution of the system into two independent stages. The first stage includes the solution of the kinetic model in each compartment without taking into account the contributions to metabolite concentrations resulting from the movement of the blood. The second stage calculates corrections to metabolite concentrations resulting from the movement of the blood.

Here, we describe the calculation in detail for the first step (t_0, $t_0 + \Delta T$). At the beginning of the step (i.e., when $t = t_0$), we know all the metabolite concentrations in all compartments of the system ${C_{f,0}}^i$, where ${C_{f,0}}^i$ is the concentration of the *i-th* metabolite in compartment f at $t = t_0$. These data are supplied from the previous step in the calculation. Then, we show that within the framework of SBSA, it is possible to calculate the metabolite concentrations ${C_{f,1}}^i$ at $t_1 = t_0 + \Delta T$. In the first stage of the calculations, we solve all kinetic models numerically in all compartments during the time interval [t_0, $t_0 + \Delta T$]. As a result, we have intermediate values of the metabolite concentrations ${C_{f,1}}^i$ at $t = t_1$. In the second stage of the calculations, these intermediate concentrations ${C_{f,1}}^i$ are corrected to account for the movement of the blood and biological entities between compartments (see Eq. 8). From these calculations, we now have the required values of the metabolite concentrations ${C_{f,1}}^i$.

Table 17.2 Description of variables of model 1

Variable	Description	Initial Value (at time point zero)	Units
Timer	Auxiliary variable represents time in special function that reproduce the dynamics of dietary fat in small intestine	0	sec
F1	Auxiliary variable, that describes the increase of dietary fat in small intestine	0	Dimentionless
F2	Auxiliary variable, that describes the decrease of dietary fat in small intestine	1	Dimentionless
Dietary_Fat	Dose of dietary fat, expressed as concentration in intestine lumen at time point zero	100	μM
FA_ent	Concentration of free fatty acids in cytosole of enterocytes	0	μM
ChM	Concentration of Chylomicrons in blood	0	μM
VLDL	Concentration of VLDLs in blood	0	μM
VLDL_rem	Concentration of VLDL remnants in blood	0	μM
ChM_rem	Concentration of Chylomicron remnants in blood	0	μM
FA_flow	Concentration of free fatty acids in blood	0	μM

Kinetic models describing biochemical transformations of metabolites/particles The SBSA model consists of (i) basic (physiological) and (ii) kinetic modules. The physiological module is responsible for the description of the movement of biological fluids and the transfer of biological entities between various organs/tissues. The mathematical apparatus of the module is given by Eqs. (7) and (8). The kinetic module is responsible for the description of biochemical processes in each organ/tissue. The mathematical apparatus of the module is given by Eqs. (5) and (6). As explained in the "*Mathematical implementation of SBSA*" subsection, all biological processes in each compartment are described by a kinetic model (see Table 17.1). Different compartments can be associated with the same or different kinetic models. Therefore, the number of different kinetic models included in the kinetic module is determined by the number of different organs/tissues included in the construction of the SBSA-based model. In this section, we describe the different kinetic models associated with the SBSA model of lipid spillover. These are

Model 1: Formation of chylomicrons (ChMs) and their influx in *vena cava* from the lymphoid system through the *thoracic duct*.
Model 2: Hydrolysis of TGs of ChMs and VLDLs in adipose tissue and the release/uptake of fatty acids from/in the tissue.
Model 3: Hydrolysis of TGs of ChMs and VLDLs in muscle and the release/uptake of fatty acid from/in the tissue.
Model 4: Uptake of free FAs and FAs released from ChMs and VLDL remnants and VLDL formation in the liver.

Below, we describe the kinetic models in further detail.

Model 1 describes ChMs formation from the fat of food in enterocytes and the release of the ChMs into the blood via the lymphatic system (thoracic duct). *Model 1* includes 10 variables (see detailed description in Table 17.2), whose dynamics are

Table 17.3 Description of rate laws of model 1

Reaction	Rate Law	Comments
R1: = timer;	V(1) = k_time;	Auxiliary reaction for agreement between the times of dietary fat dynamics and the internal time of model
R2: = f1;	If *timer* > *f1_lim* then $V(2) = \text{k\_f1}$ else $V(2) = 0$	V(2) describes the increase of auxiliary variable f1
R3: = f2;	If *timer* >; *f2_lim* then $V(3) = \text{k\_f2}$ else $V(3) = 0$	V(3) describes the increase of auxiliary variable f2
R4:Dietary_Fat = FA_ent;	$V(4) = \text{k\_df\_fa*Dietary\_Fat*f2*f1}^2/(\text{Km\_f1} + \text{f1}^2)$;	Fatty acids absorption, the part of formula in bold reproduces the dietary fat dynamics in small intestine
R5:FA_ent = ;	V(5) = k_fa_cm*FA_ent;	Fatty acids inclusion in chylomicrons
R6: = ChM;	V(6) = k_fa_cm*FA_ent/N_fa_cm;	Chylomicron production
R7:VLDL = ;	V(7) = k_vldl_deg*VLDL;	VLDLs degradation in blood
R8:VLDL_rem = ;	V(8) = k_vldlr_deg*VLDL_rem;	VLDL remnants degradation in blood
R9:ChM = ;	V(9) = k_cm_deg*ChM;	Chylomicrons degradation in blood
R10:ChM_rem = ;	V(10) = k_cmr_deg*ChM_rem;	Chylomicron remnants degradation in blood
R11:FA_flow = ;	V[11] = k_fafl_deg*FA_flow;	Free Fatty Acids degradation in blood

described by the following ODE system:

$$\begin{aligned} d\text{timer}/d\text{t} &= \text{V}[1] \\ d\text{f1}/d\text{t} &= \text{V}[2] \\ d\text{f2}/d\text{t} &= \text{V}[3] \\ d\text{Dietary\_Fat}/d\text{t} &= -V[4] \\ d\text{FA\_ent}/d\text{t} &= \text{V}[4] - \text{V}[5] \\ d\text{ChM}/d\text{t} &= \text{V}[6] - \text{V}[9] \\ d\text{VLDL}/d\text{t} &= -\text{V}[7] \\ d\text{VLDL\_rem}/d\text{t} &= -\text{V}[8] \\ d\text{ChM\_rem}/d\text{t} &= -\text{V}[10] \\ d\text{FA\_flow}/d\text{t} &= -\text{V}[11], \end{aligned} \tag{17.9}$$

The right-hand sides of the system described by Eq. (9) are given by the rate laws listed in Table 17.3. The values of the rate law parameters are listed in Table 17.4.

Model 2 describes FA exchange in capillaries of adipose tissue. *Model 2* includes 10 variables (see detailed description in Table 17.5), whose dynamics are described by the following ODE system:

$$\begin{aligned} d\text{FA\_flow}/d\text{t} &= -\text{V}[1] \\ d\text{FA\_exch}/d\text{t} &= \text{V}[1] - \text{V}[2] + \text{V}[3] + \text{V}[7] + \text{V}[9] \\ d\text{FA\_stor}/d\text{t} &= \text{V}[2] - \text{V}[3] \end{aligned}$$

Table 17.4 Description of parameters of model 1

Parameter	Description	Value	Units
k_time	Auxiliary coefficient of agreement between the times of dietary fat dynamics and the internal time of model	1	Dimensionless
k_f1	Auxiliary coefficient of rate of increase of dietary fat in small intestine after fat load	1	Dimensionless
f1_lim	Time after fat load, when the f1 variable stops to increase	60	sec
k_f2	Auxiliary coefficient of rate of decrease of dietary fat in small intestine after fat load	1	Dimensionless
f2_lim	Time after fat load, when the f2 variable stops to increase	7200	sec
k_df_fa	Rate constant of fatty acids absorptions from small intestine to enterocytes	1	1/sec
Km_f1	Concentration of fatty acids in intestine lumen, that causes half-maximal rate of absorption (EC50)	1	mM
N_fa_cm	Number of fatty acids molecules in one chylomicrons	10000	Molecules/ particle
k_fa_cm	Rate constant of fatty acids inclusion in chylonicrons (chylomicrons production)	1	1/sec
k_vldl_deg	Rate constant of VLDLs degradation in blood	0	1/sec
k_vldlr_deg	Rate constant of VLDL remnants degradation in blood	0	1/sec
k_cm_deg	Rate constant of Chylomicrons degradation in blood	0	1/sec
k_cmr_deg	Rate constant of Chylomicron remnants degradation in blood	0	1/sec
k_fafl_deg	Rate constant of Free Fatty Acids degradation in blood	0	1/sec

Table 17.5 Description of variables of model 2

Variable	Description	Initial Value (at time point zero)	Units
FA_flow	Concentration of free fatty acids in blood	0	μM
FA_exch	Concentration of free fatty acids in proteoglycan matrix	0	μM
FA_stor	Concentration of stored fatty acids in adipocytes	0	μM
ChM	Concentration of Chylomicrons in blood	0	μM
BS	Concentration of binding sites on endothelium for VLDLs and Chylomicrons	5	μM
VLDL	Concentration of VLDLs in blood	0	μM
ChM_rem	Concentration of Chylomicron remnants in blood	0	μM
VLDL_rem	Concentration of VLDL remnants in blood	0	μM

$$
\begin{aligned}
d\mathrm{ChM}/d\mathrm{t} &= -\mathrm{V}[4] \\
d\mathrm{BS}/d\mathrm{t} &= -\mathrm{V}[4] - \mathrm{V}[5] + \mathrm{V}[6] + \mathrm{V}[8] \\
d\mathrm{ChM\_BS}/d\mathrm{t} &= \mathrm{V}[4] - \mathrm{V}[6] \\
d\mathrm{VLDL}/d\mathrm{t} &= -\mathrm{V}[5] \\
d\mathrm{VLDL\_BS}/d\mathrm{t} &= \mathrm{V}[5] - \mathrm{V}[8] \\
d\mathrm{ChM\_rem}/d\mathrm{t} &= \mathrm{V}[6] \\
d\mathrm{VLDL\_rem}/d\mathrm{t} &= \mathrm{V}[8],
\end{aligned}
\tag{17.10}
$$

Table 17.6 Description of rate laws of model 2

Reaction	Rate law	Comments
R1:FA_flow = FA_exch;	V(1) = k_fa_tr_fl_ex*FA_flow-k_fa_tr_ex_fl*FA_exch;	Free fatty acids exchange between blood plasma and proteoglycan matrix
R2:FA_exch = FA_stor;	V(2) = k_fa_uptake*FA_exch;	Free fatty acids uptake by adipoytes
R3:FA_stor = FA_exch;	If *FA_stor* > *FA_stor_lim* then *V*(3) = *k_fa_release* else *V*(3) = *k_fa_release*FA_stor/FA_stor_lim*	Rate of fatty acids mobilisation from adipocytes is not depend on concentration of stored fatty acids (first order reaction) if this concentration is under lower limit (FA_stor_lim). Otherwise, this rate is limited with lack of stored fatty acids
R4:ChM + BS = ChM_BS;	V(4) = k_cm_bs*ChM*BS;	Chylomicrons binding to their binding sites on endothelium
R5:VLDL + BS = VLDL_BS;	V(5) = k_vldl_bs*VLDL*BS;	VLDLs binding to their binding sites on endothelium
R6:ChM_BS = BS + ChM_rem;	V(6) = k_cm_hyd*ChM_BS*LPL;	Triglyceride hydrolysis by lipoprotein lipase (LPL) and Chylomicron remnants formation
R7: = FA_exch;	V(7) = k_cm_hyd*ChM_BS*LPL*(N_fa_cm-N_fa_cmr);	Triglyceride hydrolysis by lipoprotein lipase (LPL) and fatty acids release from Chylomicrons
R8:VLDL_BS = BS + VLDL_rem;	V(8) = k_vldl_hyd*VLDL_BS*LPL;	Triglyceride hydrolysis by lipoprotein lipase (LPL) and VLDL remnants formation
R9: = FA_exch;	V(9) = k_vldl_hyd*VLDL_BS*LPL*(N_fa_vldl-N_fa_vldlr);	Triglyceride hydrolysis by lipoprotein lipase (LPL) and fatty acids release from VLDL

The right-hand sides of the system described by Eq. (10) are given by rate laws listed in Table 17.6. The values of the rate law parameters are listed in Table 17.7.

Model 3 describes FA exchange in capillaries of muscles. *Model 3* includes 10 variables (see detailed description in Table 17.8) whose dynamics are described by the following ODE system:

$$\begin{aligned}
d\text{FA_flow}/d\text{t} &= -\text{V}[1] \\
d\text{FA_exch}/d\text{t} &= \text{V}[1] - \text{V}[2] + \text{V}[3] + \text{V}[7] + \text{V}[9] \\
d\text{FA_stor}/d\text{t} &= \text{V}[2] - \text{V}[3] \\
d\text{ChM}/d\text{t} &= -\text{V}[4] \\
d\text{BS}/d\text{t} &= -\text{V}[4] - \text{V}[5] + \text{V}[6] + \text{V}[8] \\
d\text{ChM_BS}/d\text{t} &= \text{V}[4] - \text{V}[6] \\
d\text{VLDL}/d\text{t} &= -\text{V}[5] \\
d\text{VLDL_BS}/d\text{t} &= \text{V}[5] - \text{V}[8] \\
d\text{ChM_rem}/d\text{t} &= \text{V}[6] \\
d\text{VLDL_rem}/d\text{t} &= \text{V}[8],
\end{aligned} \tag{17.11}$$

Table 17.7 Description of parameters of model 2

Parameters	Description	Value	Units
k_fa_tr_fl_ex	Rate constant of free fatty acids transport from blood plasma to proteoglycan matrix	1	1/sec
k_fa_tr_ex_fl	Rate constant of free fatty acids transport from proteoglycan matrix to blood plasma	1	1/sec
k_fa_uptake	Rate constant of free fatty acids absorption from proteoglycan matrix by adipocytes	1	1/sec
k_fa_release	Rate constant of free fatty acids release from adipocytes to proteoglycan matrix	0	1/sec
FA_stor_lim	Minimal concentration of stored free fatty acids in adipocytes that not limited fatty acids release	1	μM
k_cm_bs	Rate constant of Chylomicrons binding to their binding sites on endothelium	1	1/sec
k_vldl_bs	Rate constant of Chylomicrons binding to their binding sites on endothelium	1	1/sec
k_cm_hyd	Rate constant of triglyceride hydrolysis by lipoprotein lipase (LPL) and fatty acids release from Chylomicrons	1	1/sec
k_vldl_hyd	Rate constant of triglyceride hydrolysis by lipoprotein lipase (LPL) and fatty acids release from Chylomicrons	1	1/sec
LPL	Lipoprotein lipase (LPL) concentration	10	μM
N_fa_cm	Number of fatty acids molecules in one chylomicron	10000	Molecules/particle
N_fa_cmr	Number of fatty acids molecules in one chylomicron remnant	100	Molecules/particle
N_fa_vldl	Number of fatty acids molecules in one VLDL	5000	Molecules/particle
N_fa_vldlr	Number of fatty acids molecules in one VLDL remnant	100	Molecules/particle

Table 17.8 Description of variables of model 3

Variable	Description	Initial Value (at time point zero)	Units
FA_flow	Concentration of free fatty acids in blood	0	μM
FA_exch	Concentration of free fatty acids in proteoglycan matrix	0	μM
FA_stor	Concentration of stored fatty acids in muscle cells	0	μM
ChM	Concentration of Chylomicrons in blood	0	μM
BS	Concentration of binding sites on endothelium for VLDLs and Chylomicrons	5	μM
VLDL	Concentration of VLDLs in blood	0	μM
ChM_rem	Concentration of Chylomicron remnants in blood	0	μM
VLDL_rem	Concentration of VLDL remnants in blood	0	μM

The right-hand sides of the system described by Eq. (11) are given by rate laws listed in Table 17.9. Values of the rate law parameters are listed in Table 17.10.

Table 17.9 Description of rate laws of model 3

Reaction	Rate law	Comments
R1:FA_flow = FA_exch;	V(1) = k_fa_tr_fl_ex*FA_flow-k_fa_tr_ex_fl*FA_exch;	Free fatty acids exchange between blood plasma and proteoglycan matrix
R2:FA_exch = FA_stor;	V(2) = k_fa_uptake*FA_exch;	Free fatty acids uptake by adipoytes
R3:FA_stor = ;	V(3) = k_energy_exp*FA_stor	Free fatty acids usage for energy production
R4:ChM + BS = ChM_BS;	V(4) = k_cm_bs*ChM*BS;	Chylomicrons binding to their binding sites on endothelium
R5:VLDL + BS = VLDL_BS;	V(5) = k_vldl_bs*VLDL*BS;	VLDLs binding to their binding sites on endothelium
R6:ChM_BS = BS + ChM_rem;	V(6) = k_cm_hyd*ChM_BS* LPL;	Triglyceride hydrolysis by lipoprotein lipase (LPL) and Chylomicron remnants formation
R7: = FA_exch;	V(7) = k_cm_hyd*ChM_BS* LPL*(N_fa_cm-N_fa_cmr);	Triglyceride hydrolysis by lipoprotein lipase (LPL) and fatty acids release from Chylomicrons
R8:VLDL_BS = BS + VLDL_rem;	V(8) = k_vldl_hyd*VLDL_BS* LPL;	Triglyceride hydrolysis by lipoprotein lipase (LPL) and VLDL remnants formation
R9: = FA_exch;	V(9) = k_vldl_hyd*VLDL_BS* LPL*(N_fa_vldl-N_fa_vldlr);	Triglyceride hydrolysis by lipoprotein lipase (LPL) and fatty acids release from VLDL

Table 17.10 Description of parameters of model 3

Parameters	Description	Value	Units
k_fa_tr_fl_ex	Rate constant of free fatty acids transport from blood plasma to proteoglycan matrix	1	1/sec
k_fa_tr_ex_fl	Rate constant of free fatty acids transport from proteoglycan matrix to blood plasma	1	1/sec
k_fa_uptake	Rate constant of free fatty acids absorption from proteoglycan matrix by adipocytes	1	1/sec
k_energy_exp	Rate constant of free fatty acids usage for energy production	0	1/sec
k_cm_bs	Rate constant of Chylomicrons binding to their binding sites on endothelium	1	1/sec
k_vldl_bs	Rate constant of Chylomicrons binding to their binding sites on endothelium	1	1/sec
k_cm_hyd	Rate constant of triglyceride hydrolysis by lipoprotein lipase (LPL) and fatty acids release from Chylomicrons	1	1/sec
k_vldl_hyd	Rate constant of triglyceride hydrolysis by lipoprotein lipase (LPL) and fatty acids release from Chylomicrons	1	1/sec
LPL	Lipoprotein lipase (LPL) concentration	10	μM
N_fa_cm	Number of fatty acids molecules in one chylomicron	10000	Molecules/particle
N_fa_cmr	Number of fatty acids molecules in one chylomicron remnant	100	Molecules/particle
N_fa_vldl	Number of fatty acids molecules in one VLDL	5000	Molecules/particle
N_fa_vldlr	Number of fatty acids molecules in one VLDL remnant	100	Molecules/particle

Table 17.11 Description of variables of model 4

Variables	Description	Initial Value (at time point zero)	Units
ChM_rem	Concentration of Chylomicron remnants in blood, expressed as concentration of included fatty acids	0	μM
FA_liv	Concentration of free fatty acids in hepatocytes	0	μM
VLDL_rem	Concentration of VLDL remnants in blood, expressed as concentration of included fatty acids	0	μM
FA_flow	Concentration of free fatty acids in blood	0	μM
VLDL	Concentration of VLDLs in blood, expressed as concentration of included fatty acids	0	μM
ChM	Concentration of Chylomicrons in blood, expressed as concentration of included fatty acids	0	μM

Table 17.12 Description of rate laws of model 4

Reaction	Rate laws	Comments
R1:ChM_rem = ;	V(1) = k_cmr_upt*ChM_rem;	Chylomicron remnants uptake by hepatocytes
R2: = FA_liv;	V(2) = k_cmr_upt*ChM_rem* N_fa_cmr;	Uptake of free fatty acids from Chylomicron remnants
R3:VLDL_rem = ;	V(3) = k_vldlr_upt*VLDL_rem;	VLDL remnants uptake by hepatocytes
R4: = FA_liv;	V(4) = k_vldlr_upt*VLDL_rem* N_fa_vldlr;	Uptake of free fatty acids from VLDL remnants
R5:FA_flow = FA_liv;	V(5) = k_fa_upt*FA_flow;	Free fatty acids uptake by hepatocytes
R6:FA_liv = ;	V(6) = k_fa_energy*FA_liv;	Free fatty acids usage for energy production (beta-oxidation)
R7:FA_liv = ;	V(7) = k_fa_vldl_syn*FA_liv;	Fatty acids inclusion in VLDLs
R8: = VLDL;	V(8) = k_fa_vldl_syn*FA_liv/ N_fa_vldl;	VLDL production
R9:ChM = ;	V(9) = k_cm_deg*ChM;	Chylomicrons degradation in blood

Model 4 describes FA exchange in liver tissue. *Model 4* includes 6 variables (see detailed description in Table 17.11) whose dynamics are described by the following ODE system:

$$\begin{aligned} d\text{ChM\_rem}/d\text{t} &= -\text{V}[1] \\ d\text{FA\_liv}/d\text{t} &= \text{V}[2] + \text{V}[4] + \text{V}[5] - \text{V}[6] - \text{V}[7] \\ d\text{VLDL\_rem}/d\text{t} &= -\text{V}[2] \\ d\text{FA\_flow}/d\text{t} &= -\text{V}[5] \\ d\text{VLDL}/d\text{t} &= \text{V}[7] \\ d\text{ChM}/d\text{t} &= -\text{V}[9], \end{aligned} \tag{17.12}$$

The right-hand sides of the system described by Eq. (12) are given by rate laws listed in Table 17.12. Values of rate law parameters are listed in Table 17.13.

Each of the models of the kinetic module has been associated with compartments of the physiological module (see Table 17.1).

Table 17.13 Description of parameters of model 4

Parameters	Description	Value	Units
k_cmr_upt	Rate constant of Chylomicron remnants uptake by hepatocytes	1	1/sec
N_fa_cmr	Number of fatty acids molecules in one chylomicron remnant	100	Molecules/particle
k_vldlr_upt	Rate constant of VLDL remnants uptake by hepatocytes	1	1/sec
N_fa_vldlr	Number of fatty acids molecules in one VLDL remnant	100	Molecules/particle
k_fa_upt	Rate constant of free fatty acids uptake by hepatocytes	1	1/sec
k_fa_energy	Rate constant of free fatty acids usage for energy production (beta-oxidation)	0.1	1/sec
k_fa_vldl_syn	Rate constant of VLDL production	1	1/sec
N_fa_vldl	Number of fatty acids molecules in one VLDL	5000	Molecules/particle
k_cm_deg	Rate constant of Chylomicrons degradation in blood	0	1/sec

17.4 Outcome of the Model

Comparison of SBSA with CAT/ACAT algorithm In this section, we compare two different algorithms used to describe the movement of biological entities with blood flow through blood vessels. These are the CAT/ACAT algorithm (Huang et al. 2009) and the SBSA presented in this chapter.

The CAT/ACAT algorithm was initially developed to describe the absorption and transit of non-degradable and highly soluble drugs in the gastrointestinal tract (Agoram et al. 2001; Grass 1997). The process of a drug passing through the small intestine is considered as a flow through a series of segments. Each segment can be described as a single compartment with linear transfer kinetics. Each compartment can have different volumes and flow-rates, but they all have the same transit rate constant. CAT/ACAT (or similar) algorithms have been implemented in various software packages (simulations-plus.com 2012; system-biology.com 2012).

SBSA was developed to describe fast processes that occur in the bloodstream (or other flowing biological fluids). The term "fast process" refers to processes that result in a change in the concentration of some metabolite (or any other biological entity) located in blood with a characteristic time less than the turnover time of the circulatory system. An example of a fast process is the exchange of oxygen and carbon dioxide between erythrocytes and tissues in the bloodstream. The blood in arterioles is oxygen-rich and the blood in venules is saturated with carbon dioxide. This means that the O_2/CO_2 ratio decreases significantly from the beginning of the capillaries to their ends. This spatial distribution of the O_2/CO_2 ratio is provided by fast O_2/CO_2 exchange in capillaries. SBSA was developed for the purpose of describing the spatially non-homogeneous distribution of biological entities.

To compare the SBSA and CAT/ACAT algorithm we selected a model describing the movement of a portion of blood through a tissue. Blood transports

non-homogeneously distributed biological entities. We assumed that within the framework of the model, during the movement, the biological entity could interact with the tissue. Chylomicrons (ChM) are considered to be biological entities transported within the bloodstream. Adipose tissue was selected as a tissue through which ChMs are transported. In accordance with description in sub-section "Lipid spillover" of the section "Modeling framework – description of biological system and model requirements," ChMs circulating in blood are able to attach to endothelial cells that pave the capillaries of adipose tissue. To account for the process in our model, we assumed that the rate of attachment of ChMs to the cells is described in accordance with the irreversible mass action law with a corresponding binding rate constant (k_cm_bs):

$$\text{v\_sorption} = \text{k\_cm\_bs}*[\text{ChM}]*[\text{BS}],$$

where BS is the concentration of binding sites for ChMs or VLDLs located on the surface of the endothelium wall.

The value of the rate constant ($\text{k\_cm\_bs} = 0.008\ \text{s}^{-1}$) was selected so as to provide a 20 % attachment of ChMs to the endothelial cells paving the capillaries of adipose tissue during a single passage through the part of adipose tissue considered in the model. This is in line with experimental results of measurements of arterio-venous differences in ChM concentration across subcutaneous adipose tissue and skeletal muscle *in vivo* (Evans et al. 1999).

The initial distribution of ChMs (i.e., dependence of ChM concentration on spatial coordinate or compartment number) was selected in the following way. Dependence of ChM concentration is bell-shaped for the first 16 compartments of the model and equal to zero for all other compartments.

On the basis of the model, we determine the answers to the following questions:

- Does the shape of the spatial distribution change over time?
- How does the ChM concentration change in blood? Is this change fully determined by the value of *k_cm_bs*?

We answered these questions by applying the SBSA and CAT/ACAT algorithm to the model described above. This means that the movement of the portion of blood through the vessel and the distribution of the concentration of ChMs at each moment of time was modeled and simulated in accordance with these algorithms. To simulate the dependence of ChM concentration on time and compartment number (spatial coordinate) within the framework of the SBSA, we applied the model described in the "Model development" section. To compare the results obtained from the framework of the SBSA-based model with those obtained from the CAT/ACAT algorithm, we simulated the passage of ChMs through the "adipose" route in the SBSA-based model. In accordance with the data given in Table 17.1 and Fig. 17.1, this route includes 56 compartments.

To simulate the dependence of ChM concentration on time and compartment number within the framework of the CAT/ACAT algorithm, we applied the model

described below:

$$
\begin{aligned}
d\mathbf{ChM_1}/d\mathbf{t} &= -k\_transport^{*}[ChM_1],\\
d\mathbf{ChM_i}/d\mathbf{t} &= k\_transport^{*}\left[ChM_{i-1}\right] - k\_transport^{*}\left[ChM_i\right], \mathrm{i} = 2, \ldots 12\\
d\mathbf{ChM}i/d\mathbf{t} &= k\_transport^{*}\left[\mathrm{ChM_{i-1}}\right] - k\_transport^{*}\left[\mathrm{ChM_i}\right]\\
&\quad - k\_cm\_bs^{*}\left[\mathrm{ChM_i}\right], \mathrm{i} = 13, \ldots 44,\\
d\mathbf{ChM_i}/d\mathbf{t} &= k\_transport^{*}\left[\mathrm{ChM_{i-1}}\right] - k\_transport^{*}\left[\mathrm{ChM_i}\right], \mathrm{i} = 45, \ldots, 55\\
d\mathbf{ChM_{56}}/d\mathbf{t} &= k\_transport^{*}[\mathrm{ChM_{55}}],
\end{aligned}
$$

where *k_transport* is the rate constant of ChM transport from the upstream compartment to the downstream one. It is worth noting that values of the parameters responsible for the transport of ChMs between compartments, within the framework of the CAT/ACAT model, were selected so as to provide an exact match of the time of passage of ChMs through the adipose tissue in the CAT/ACAT model with the time of blood flow passage through adipose tissue within the framework of the SBSA model (which is equal to 56 s):

$$k\_transport = 1\mathrm{s}^{-1}$$

Simulation results obtained within the framework of the SBSA and CAT/ACAT algorithm are shown in Figs. 17.2 and 17.3. The following differences between simulations were identified:

(1) Despite the decrease in the maximal value of ChM concentration with the compartment number, the shape of the time profile of ChM concentration calculated in various compartments did not change in the SBSA-based model (Fig. 17.2a). On the contrary, we observed a broadening of the time profile in the CAT/ACAT algorithm-based model (Fig. 17.2b). In fact, ChMs were distributed among 40 compartments at $t = 30$ s, although they were initially distributed among only 17 compartments (Fig. 17.3).
(2) The value of ChM concentration at the peak of the time dynamics decreased by 20 % with an increase in compartment number in the SBSA-based model (Fig. 17.2a). In the CAT/ACAT algorithm-based mode (Fig. 17.2b), we observed a more significant decrease (more than two times the initial level of ChMs) in the concentration.

In accordance with clause (2), we can state that the decrease in ChM concentration resulting from the single passage of the selected portion of blood through adipose tissue, calculated within the framework of the CAT/ACAT algorithm, is significantly more than that calculated on the basis of the SBSA. To understand the nature of the significant differences in simulation results produced by the CAT/ACAT and SBSA-based models, we simulated the spatial-temporal distribution of ChM concentration under the condition of absence of ability of ChMs to attach to the endothelial cells, i.e., we assumed the value of $k\_cm\_bs = 0$. Evidently, under these conditions, the concentration of ChMs during the movement with blood flow cannot decrease since there is no process for ChM consumption in the model. The results shown in Fig. 17.4a

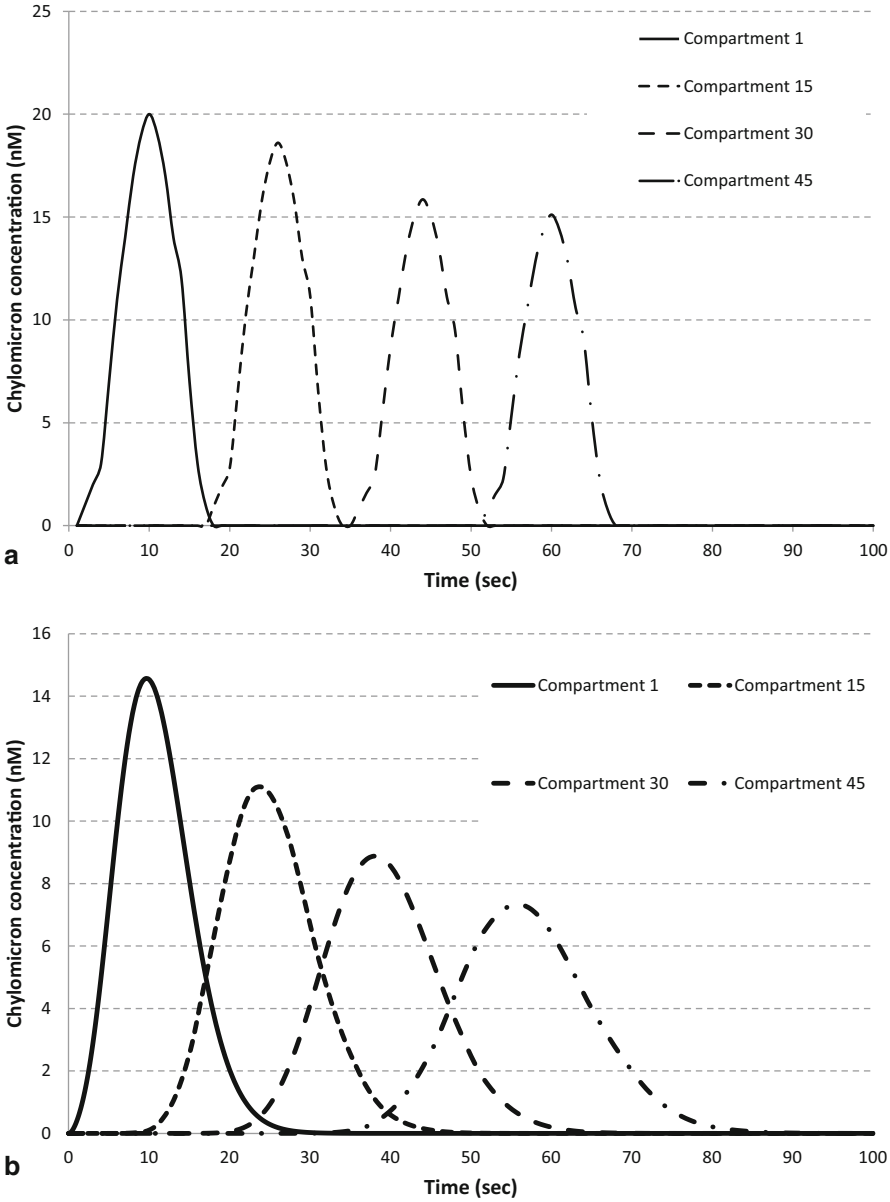

Fig. 17.2 Simulations of time courses of ChM concentration for various compartments of the "Adipose" route. Simulations were performed to compare models developed within the framework of the SBSA (**a**) with those of the CAT/ACAT algorithm (**b**). All initial values and parameters were identical for both versions of the model. In both the models, the "Adipose" route was considered. The route consisted of 56 compartments. At the $t = 0$, a bell-shaped distribution of ChMs was observed in 12 upstream compartments located immediately before the start of the "Adipose" route. In both CAT/ACAT and SBSA-based models, the initial concentration of ChMs in any of the 56 compartments of the "Adipose" route was zero. Time courses for ChM concentration were calculated in the 1st, 10th, 20th, 30th, 40th, and 50th compartments of the "Adipose" route. The kinetic parameter responsible for binding ChMs to the vessel wall cells was equal to 0.08 s^{-1}

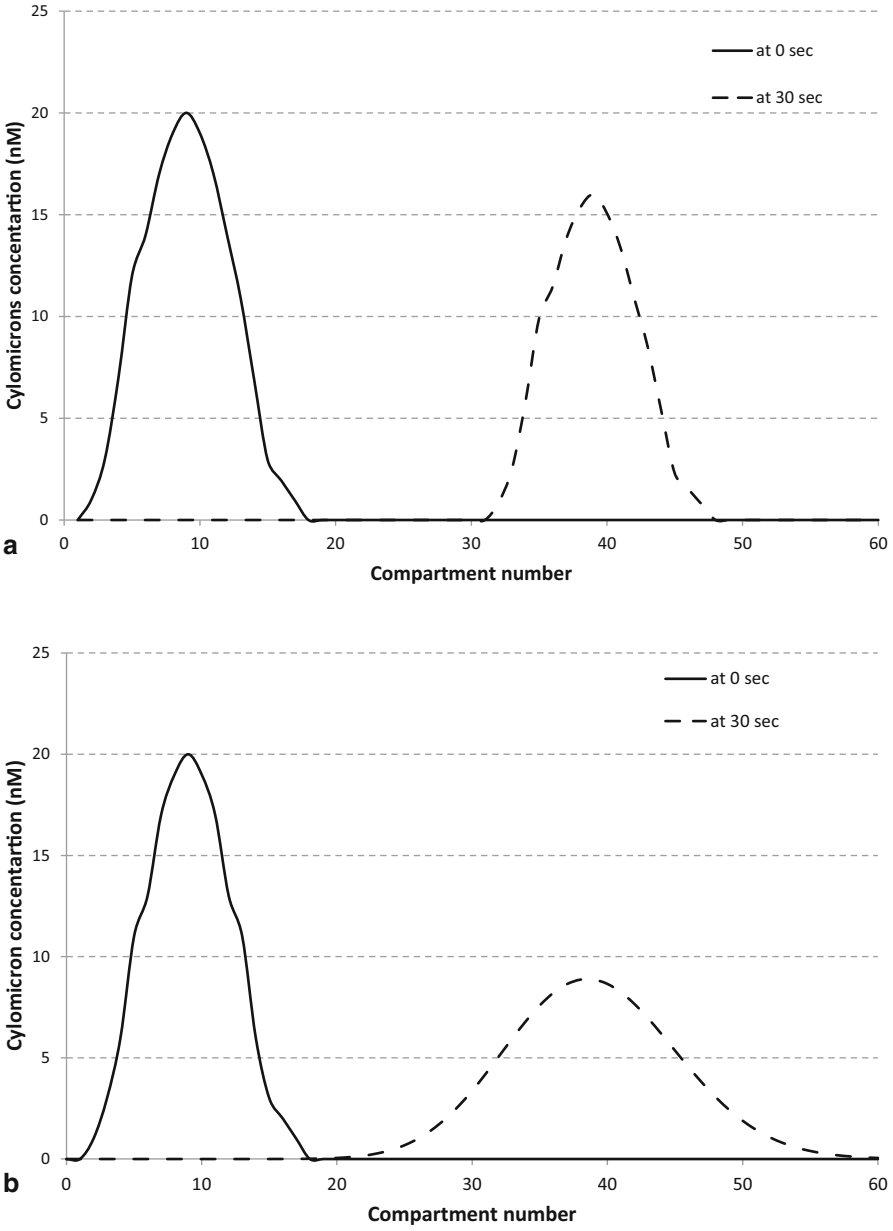

Fig. 17.3 Simulations of spatial distribution of ChM concentration along the "Adipose" route. Simulations were performed to compare models developed within the framework of the SBSA (**a**) with those of the CAT/ACAT algorithm (**b**). All initial values and parameters were identical for both versions of the model. In both models, the "Adipose" route was considered. The route consisted of 56 compartments. At $t = 0$, a bell-shaped distribution of ChMs was observed in the first 17 compartments of the "Adipose" route. The maximum concentration of ChMs was equal to 20 nM. The peak of the initial distribution corresponded to the 9^{th} compartment. The spatial distribution of ChM concentration along the "Adipose" route was simulated for an initial time $t = 0$ (*solid curve*) and $t = 30$ s (*dashed curve*). We assumed that the kinetic parameter responsible for the binding of ChMs to the vessel wall cells was equal to 0.08 s^{-1}

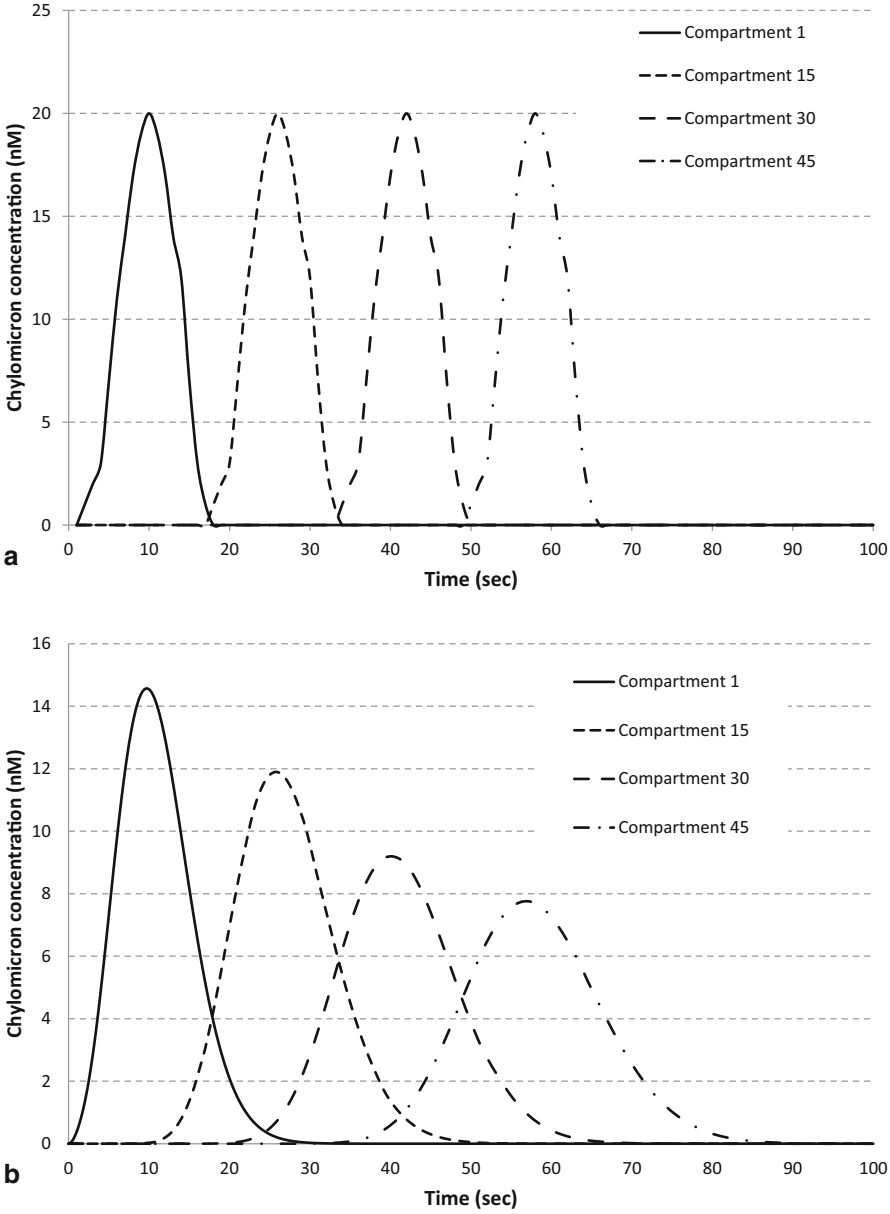

Fig. 17.4 Time course simulations of ChM concentration for various compartments of the "Adipose" route. Simulations were performed to compare models developed within the framework of the SBSA (**a**) with those of the CAT/ACAT algorithm (**b**). All initial values and parameters were identical for both versions of the model. In both the models, the "Adipose" route was considered. The route consisted of 56 compartments. At $t = 0$, a bell-shaped distribution of ChMs was observed in the 12 upstream compartments located immediately before the start of the "Adipose" route. In both CAT/ACAT and SBSA-based models, the initial concentration of ChMs in any of the 56 compartments of the "Adipose" route was zero. Time courses for ChM concentration were calculated in the 1st, 10th, 20th, 30th, 40th, and 50th compartments of the "Adipose" route. The kinetic parameter responsible for binding ChMs to the vessel wall cells was 0

demonstrate that simulations obtained within the framework of the SBSA-based model are in line with the conclusion. In fact, there is no decrease in the peak value of the time series of ChM concentration calculated for various compartments and the shape of the time profile does not change with an increase in compartment number. However, the simulations obtained within the framework of CAT/ACAT algorithm-based model (Fig. 17.4b) demonstrate both a significant decrease in the peak value of the time series of ChM concentration with an increase in compartment number and a broadening of the time profile with an increase in compartment number. By comparing Fig. 17.2b and 17.4b, we can conclude that the time series of ChM concentrations calculated in various compartments do not depend significantly on the ability of ChMs to attach to the endothelial cells, and this has been taken into account in the CAT/ACAT model. Even under the condition of $k\_cm\_bs = 0$, a significant decrease in the peak value of ChM concentrations and a broadening of the time profile is observed with an increase in compartment number.

This means that the CAT/ACAT algorithm cannot be used to describe the dynamics of the movement of any biological entity with blood flow. In contrast, the SBSA-based model enables us to correctly simulate both the movement of a biological entity with blood flow and the dynamic changes in its concentration resulting from chemical reactions or interactions with cells of the vessel wall. Hence, we propose using the SBSA to model the dynamics of lipid spillover.

Prediction of spatial distribution of FAs and lipoproteins in adipose and liver tissues In this section, we illustrate how the SBSA-based model of lipid spillover can describe the time dynamics of free FAs, ChMs, and ChMRs in the selected portion of blood passing through various blood vessels located in adipose tissue and liver tissue.

In our SBSA-based model, adipose tissue is described by 56 compartments and the residence time of a portion of blood is estimated as 50.4 s (see Table 17.1). Figure 17.5 shows the simulation of time dynamics of free FAs, ChMs, and ChMRs in the selected blood portion passing through adipose tissue. At $t = 0$, the portion of blood is located at the entrance to the adipose arteries and contains only ChMs, i.e., the concentration of free FAs and ChMRs is zero. Then, the blood portion sequentially passes through the adipose arteries (from 0 to 11 s), adipose capillaries (from 12 to 45 s), and adipose veins (from 46 to 50.4 s). The simulation results show that the concentrations of free FAs, ChMs, and ChMRs do not change when blood passes through the arteries and veins, but when it passes through the capillaries of adipose tissue, there is a decrease in the concentration of ChMs in the blood. This can be explained in terms of the hydrolysis of the TGs of ChMs by LPL (see also Chap. 2.6). LPL catalyzes the production of free FAs and ChMRs from ChMs, and in fact, it was seen that the concentrations of free FAs and ChMRs in the blood increased as they passed through the capillaries of adipose tissue. It was also observed that as the passage time for the portion of blood increased through the capillaries of adipose tissue, the changes in the concentrations of free FAs, ChMRs, and ChMs became more pronounced.

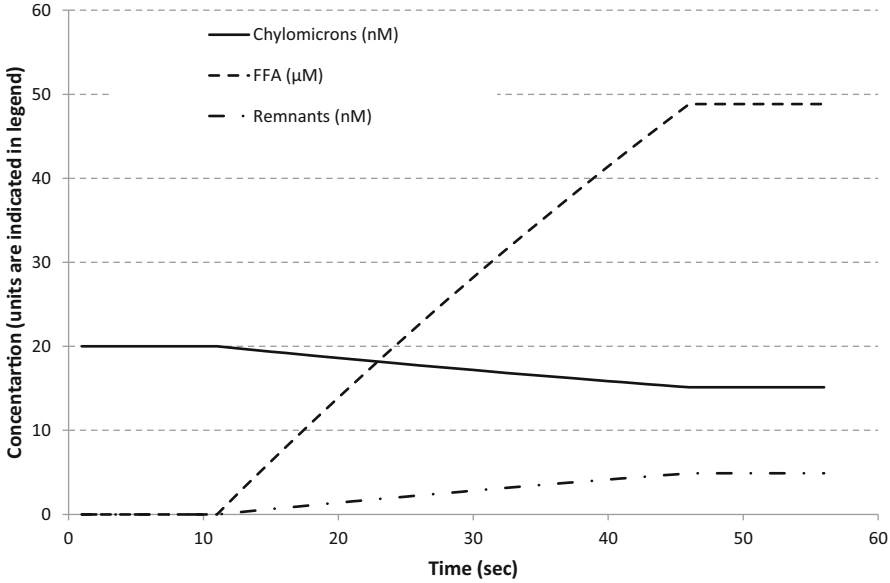

Fig. 17.5 Spillover of fatty acids from chylomicrons to FFA fraction in adipose tissue. These simulations represent the dynamics of the concentration of ChMs, ChMRs, and free FAs in the blood portion flowing along the "Adipose" route. We selected the portion of the blood located in the first compartment of the "Adipose" route at $t = 0$. Initial concentrations of ChMs, ChMRs, and free FAs in the blood portion are equal to 20 nM, 0.0 nM, and 0.0 μM, respectively. Concentrations of all other molecules/particles were assumed to be equal to zero. With each cardiac beat (i.e., each second), the portion of blood is transported to the next downstream compartment. Graphs represent changes in ChM, ChMR, and free FA concentrations in the blood portion flowing along the "Adipose" route

In a similar manner, we simulated the time dynamics of free FAs, ChMRs, and VLDLs in the selected blood portion passing through liver tissue (see Fig. 17.6). Liver tissue can be described as 17 compartments, and the residence time of a portion of blood is estimated as 15.3 s (see Table 17.1). At $t = 0$, the portion of blood is located at the entrance to the liver arteries and contains non-zero concentrations of free FAs, ChMRs, and VLDLs. Then, the blood portion sequentially passes through the liver arteries (from 0 to 3 s), liver capillaries (from 4 to 13 s), and liver veins (from 14 to 15.3 s). The simulation results show that the concentrations of free FAs, ChMRs, and VLDLs do not change when blood passes through the arteries and veins, but passage through the capillaries of liver enriches the blood with VLDLs and decreases concentrations of free FAs and ChMRs. This can be explained in terms of the absorption of free FAs and ChMRs by hepatocytes (see also Chap. 2.6). Hepatocytes use the absorbed FAs and ChMRs to assemble VLDLs with subsequent release to the blood stream. It was seen that the concentration of VLDLs increased as the blood passed through the capillaries of liver tissue. It was also observed that as the passage time for the portion of the blood increased through the capillaries of liver tissue, the changes in the concentrations of free FAs, ChMRs, and VLDLs became more pronounced.

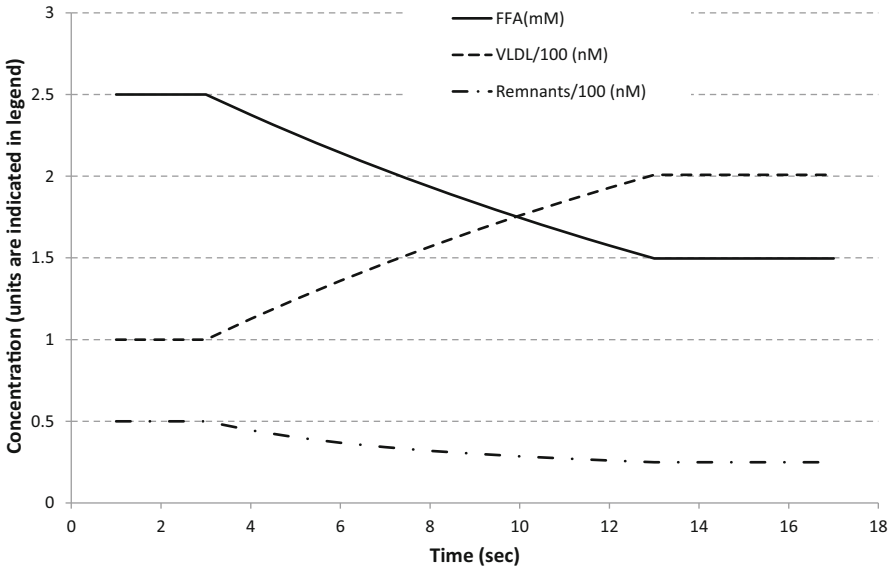

Fig. 17.6 Spillover of fatty acids from FFA fraction and chylomicron remnants to VLDL in liver. These simulations represent the dynamics of the concentrations of VLDLs, VLDLRs, and free FAs in the blood portion flowing along the "Liver" route. We selected the portion of blood located in the first compartment of the "Liver" route at $t = 0$. Initial concentrations of the VLDLs, VLDLRs, and free FAs in the blood portion are equal to 100 nM, 50 nM, and 2.5 mM, respectively. Concentrations of all other molecules/particles were assumed to be equal to zero. With each cardiac beat (i.e., each second), the portion of blood is transported to the next downstream compartment. Graphs represent changes in VLDL, VLDLR, and free FA concentrations in the blood portion flowing along the "Liver" route

17.5 Conclusions

A new algorithm was developed, which enabled us to combine kinetic models describing changes in metabolite (lipoprotein) concentrations that occurred due to biochemical transformations in blood and tissues, with the mathematical model of the molecular movement in blood flow. The algorithm may be applied to integrate a variety of experimental data and to understand the regulatory mechanisms underlying MetS development and progression.

Acknowledgements This work was supported by the FP7 ETHERPATHS project (Grant Number 222639).

References

Agoram B, Woltosz WS, Bolger MB (2001) Predicting the impact of physiological and biochemical processes on oral drug bioavailability. Adv Drug Deliv Rev 50(1):41–67

Albu JB, Heilbronn LK, Kelley DE, Smith SR, Azuma K, Berk ES, Pi-Sunyer FX, Ravussin E (2010) Look AHEAD Adipose research group. Metabolic changes following a 1-year diet and exercise intervention in patients with type 2 diabetes. Diabetes 59(3):627–633

Armoni M, Harel C, Karnieli E (2007) Transcriptional regulation of the GLUT4 gene: from PPAR-gamma and FOXO1 to FFA and inflammation. Trends Endocrinol Metab 18(3):100–107

Bajaj M, Pratipanawatr T, Berria R, Pratipanawatr W, Kashyap S, Cusi K, Mandarino L, DeFronzo RA (2002) Free fatty acids reduce splanchnic and peripheral glucose uptake in patients with type 2 diabetes. Diabetes 51(10):3043–3048

Czech A, Tatoń J, Piatkiewicz P (2010) Cellular glucose transport disturbances in the pathogenesis and therapy of type 2 diabetes mellitus. Endokrynol Pol 61(3):292–302

Evans K, Clark ML, Frayn KN (1999) Effects of an oral and intravenous fat load on adipose tissue and forearm lipid metabolism. Am J Physiol 276(2 Pt 1):241–248

Everett-Grueter C, Edgerton DS, Donahue EP, Vaughan S, Chu CA, Sindelar DK, Cherrington AD (2006) The effect of an acute elevation of NEFA concentrations on glucagon-stimulated hepatic glucose output. Am J Physiol Endocrinol Metab 291(3):449–459

Felber JP, Golay A (2002) Pathways from obesity to diabetes. Int J Obes Relat Metab Disord 26(2):39–45

Golay A, Felber JP, Meyer HU, Curchod B, Maeder E, Jéquier E (1984) Study on lipid metabolism in obesity diabetes. Metabolism 33(2):111–116

Grass G (1997) Simulation-models to predict oral-drug absorption from in-vitro data. Advanced Drug Delivery Review 23(1–3):199–219

He M, Su H, Gao W, Johansson SM, Liu Q, Wu X, Liao J, Young AA, Bartfai T, Wang MW (2010) Reversal of obesity and insulin resistance by a non-peptidic glucagon-like peptide-1 receptor agonist in diet-induced obese mice. PLoS One 5(12):e14205

Hirasawa A, Tsumaya K, Awaji T, Katsuma S, Adachi T, Yamada M, Sugimoto Y, Miyazaki S, Tsujimoto G (2005) Free fatty acids regulate gut incretin glucagon-like peptide-1 secretion through GPR120. Nat Med 11(1):90–94

Huang W, Lee SL, Yu LX (2009) Mechanistic approaches to predicting oral drug absorption. AAPS J 11(2):217–224

Katz A, Nambi SS, Mather K, Baron AD, Follmann DA, Sullivan G, Quon MJ (2000) Quantitative insulin sensitivity check index: a simple, accurate method for assessing insulin sensitivity in humans. J Clin Endocrinol Metab 85(7):2402–2410

Kelley DE, Mandarino LJ (2000) Fuel selection in human skeletal muscle in insulin resistance: a reexamination. Diabetes 49(5):677–683

Kim JY, Wall E van de, Laplante M, Azzara A, Trujillo ME, Hofmann SM, Schraw T, Durand JL, Li H, Li G, Jelicks LA, Mehler MF, Hui DY, Deshaies Y, Shulman GI, Schwartz GJ, Scherer PE (2007) Obesity-associated improvements in metabolic profile through expansion of adipose tissue. J Clin Invest 117(9):2621–37

Lewis GF, Carpentier A, Adeli K, Giacca A (2002) Disordered fat storage and mobilization in the pathogenesis of insulin resistance and type 2 diabetes. Endocr Rev 23(2):201–229

Lin E, Davis SS, Srinivasan J, Sweeney JF, Ziegler TR, Phillips L, Gletsu-Miller N (2009) Dual mechanism for type-2 diabetes resolution after Roux-en-Y gastric bypass. Am Surg 75(6):498–502. (discussion 502–503)

Muscelli E, Mari A, Casolaro A, Camastra S, Seghieri G, Gastaldelli A, Holst JJ, Ferrannini E (2008) Separate impact of obesity and glucose tolerance on the incretin effect in normal subjects and type 2 diabetic patients. Diabetes 57(5):1340–1348

Pastucha D, Talafa V, Malincikova J, Cihalik C, Hyjanek J, Horakova D, Janout V (2010) Obesity, hypertension and insulin resistance in childhood–a pilot study. Biomed Pap Med Fac Univ Palacky, Olomouc. Czech Repub 154(1):77–81

Pigeon E, Riou ME, St-Onge J, Couillard E, Tremblay A, Marette A, Weisnagel SJ, Joanisse DR (2009) Validation of a simple index (SIisOGTT) of insulin sensitivity in a population of sedentary men. Diabetes Metab 35(5):398–403

Prentki M, Madiraju SR (2011) Glycerolipid/free fatty acid cycle and islet β-cell function in health, obesity and diabetes. Mol Cell Endocrinol 353(1–2):88–100

Schnell S, Schaefer M, Schöfl C (2007) Free fatty acids increase cytosolic free calcium and stimulate insulin secretion from beta-cells through activation of GPR40. Mol Cell Endocrinol 263(1–2):173–180

Simulations Plus, Inc. (2012) Simulations-plus. http://www.simulations-plus.com. Accessed 10 Aug 2012

Staehr P, Hother-Nielsen O, Landau BR, Chandramouli V, Holst JJ, Beck-Nielsen H (2003) Effects of free fatty acids per se on glucose production, gluconeogenesis, and glycogenolysis. Diabetes 52(2):260–267

Stannard SR, Johnson NA (2004) Insulin resistance and elevated triglyceride in muscle: more important for survival than "thrifty" genes? J Physiol 554(3):595–607

Systems Biology (2012) Systems Biology. http://www.systems-biology.com. Accessed 10 Aug 2012

Wu CZ, Pei D, Su CC, Hsiao FC, Chu YM, Lee LH, Wang K, Hsieh AT, Lin JD, Hsia TL (2010) Comparison of oral glucose insulin sensitivity with other insulin sensitivity surrogates from oral glucose tolerance tests in Chinese. Ann Acad Med Singapore 39(1):4–8